

Weierstraß-Institut
für Angewandte Analysis und Stochastik
Leibniz-Institut im Forschungsverbund Berlin e. V.

Preprint

ISSN 2198-5855

**Tunable Kerr frequency combs and temporal localized states in
time-delayed Gires–Tournois interferometers**

Christian Schelte^{1,2,3}, Alexander Pimenov⁴, Andrei G. Vladimirov⁴,

Julien Javaloyes¹, Svetlana V. Gurevich^{2,3}

submitted: November 27, 2019

¹ Departament de Física, Universitat de les Illes Balears &
Institute of Applied Computing and Community Code (IAC-3)
C/ Valldemossa km 7.5
07122 Palma de Mallorca
Spain
E-Mail: c.schelte@uib.cat

² Institute for Theoretical Physics
University of Münster
Wilhelm-Klemm-Str. 9
48149 Münster
Germany

³ Center for Nonlinear Science (CeNoS)
University of Münster
Corrensstr. 2
48149 Münster
Germany
E-Mail: gurevics@uni-muenster.de

⁴ Weierstrass Institute
Mohrenstr. 39
10117 Berlin
Germany
E-Mail: alexander.pimenov@wias-berlin.de
andrei.vladimirov@wias-berlin.de

No. 2650

Berlin 2019



2010 *Physics and Astronomy Classification Scheme*. 05.45.-a, 02.30.Ks, 42.55.Px, 42.65.Pc, 42.65.Tg.

Key words and phrases. Temporal localized states, time-delay model, large delay, Gires–Tournois interferometer, Kerr frequency combs.

A. P. and A. G. V. acknowledge the support of SFB 787 of the DFG. C. S., J. J., S. V. G. acknowledge the support of MINECO Project COMBINA (TEC2015-65212-C3-3-P) and MOVELIGHT (PGC2018-099637-B-100 AEI/FEDER UE), PRIME program of the German Academic Exchange Service (DAAD) with funds from the German Federal Ministry of Education and Research (BMBF). C. S. wishes to thank the Laser Dynamics group at WIAS Berlin for the opportunity of a research stay where part of this work was conducted. The Authors thank B. Garbin and M. Marconi for useful discussions and comments on the manuscript.

Edited by
Weierstraß-Institut für Angewandte Analysis und Stochastik (WIAS)
Leibniz-Institut im Forschungsverbund Berlin e. V.
Mohrenstraße 39
10117 Berlin
Germany

Fax: +49 30 20372-303
E-Mail: preprint@wias-berlin.de
World Wide Web: <http://www.wias-berlin.de/>

Tunable Kerr frequency combs and temporal localized states in time-delayed Gires–Tournois interferometers

Christian Schelte, Alexander Pimenov, Andrei G. Vladimirov,
Julien Javaloyes, Svetlana V. Gurevich

Abstract

In this Letter we study theoretically a new set-up allowing for the generation of temporal localized states and frequency combs. The setup is compact (a few cm) and can be implemented using established technologies, while offering tunable repetition rates and potentially high power operation. It consists of a vertically emitting micro-cavity, operated in the Gires–Tournois regime, containing a Kerr medium with strong time-delayed optical feedback as well as detuned optical injection. We disclose sets of multistable dark and bright temporal localized states coexisting on their respective bistable homogeneous backgrounds.

Introduction

Optical frequency combs are of particular interest for applications in optical fiber communication technology and high precision metrology. They appear naturally in optical systems such as passively mode-locked lasers; in particular in mode-locked vertical external-cavity surface-emitting lasers (VECSEL) [1,2]. Here, the repetition rate of a pulse train corresponds directly to the free spectral range of the modes that compose the frequency comb. Phase locked frequency combs can be created in fiber or whispering gallery mode micro-resonators under continuous wave (CW) injection. Due to the interplay between the resonator Kerr nonlinearity, the detuning, and second order chromatic dispersion, such systems can exhibit dissipative temporal localized states (TLSs) that may be used as addressable bits in all optical information storage and processing [3, 4].

The bistable response resulting from a Kerr medium allows finding bright TLSs on a lower CW background under anomalous dispersion. Oppositely, the dark counterparts exist under normal dispersion as dips in the upper CW background. Coexistence of TLSs with different widths was observed both in coupled-mode models [5, 6] and in the one-dimensional Lugiato-Lefever equation [7]. Such states have been observed experimentally in both Kerr micro-resonators and fiber loops [8,9]. Their formation can be attributed to the locking of fronts connecting two *domains* with different constant field intensities [10–12]. A similar scenario was recently predicted in parametric oscillators [13, 14]. Bright TLSs of variable width have also been found recently in a delay differential equation (DDE) model taking into account the chromatic dispersion of a fiber loop [15]. Third order dispersion was shown to stabilize dark TLSs in the anomalous dispersion regime [16] and facilitate the coexistence and hysteresis of bright and dark TLSs as demonstrated in [17, 18].

In this letter, we propose an alternative method for the generation of phase locked frequency combs with tunable repetition rate that maintains the potential of achieving the high optical power levels characteristic of VECSEL systems.

1 Model equations

We consider a monomode micro-cavity containing a nonlinear Kerr medium coupled to a long external feedback cavity under CW injection. Two possible implementations are depicted schematically in Fig. 1. Panel (a) shows a vertically emitting micro-cavity consisting of a layer of Kerr material like silicon nitride sandwiched between two distributed Bragg reflectors (DBRs) or highly reflective coatings, and a movable distant mirror creating the time delayed feedback. The transverse degrees of freedom permit spreading the power density over a wide beam waist while still allowing for efficient fiber coupling. Translating the external mirror enables tuning of the repetition rate. Interestingly, an alternative implementation could be achieved using a short and a long ring waveguide, see panel (b).

The model for the vertical cavity system can be derived following the method of [19] and reads

$$\dot{E} = [-1 + i(s|E|^2 - \delta)] E + hY, \quad (1)$$

$$Y = \eta[E(t - \tau) - Y(t - \tau)] + \sqrt{1 - |\eta|^2}Y_0, \quad (2)$$

where E and Y denote the slowly varying electromagnetic field envelopes in the micro-cavity and the external cavity, respectively. The injection field amplitude is Y_0 , and δ is the detuning of the injection with respect to the closest micro-cavity mode. The round-trip time in the external cavity is τ and time is scaled to the photon lifetime in the micro-cavity. The cavity enhancement is scaled out allowing E and Y to be of the same order of magnitude which leads to a simpler input-output relation. The output O is the combination of the intra-cavity photons transmitted by the micro-cavity and those reflected. Finally, intracavity enhanced Kerr saturation parameter s in (m^2/V^2) reads $s = [\chi_3\omega_0 W/(2n_g c)] \times [(1 + |r_2|)(1 + |r_1|)^3/((1 - |r_1||r_2|)|t_1|^2)]$ with χ_3 the Kerr coefficient, ω_0 the injection frequency,

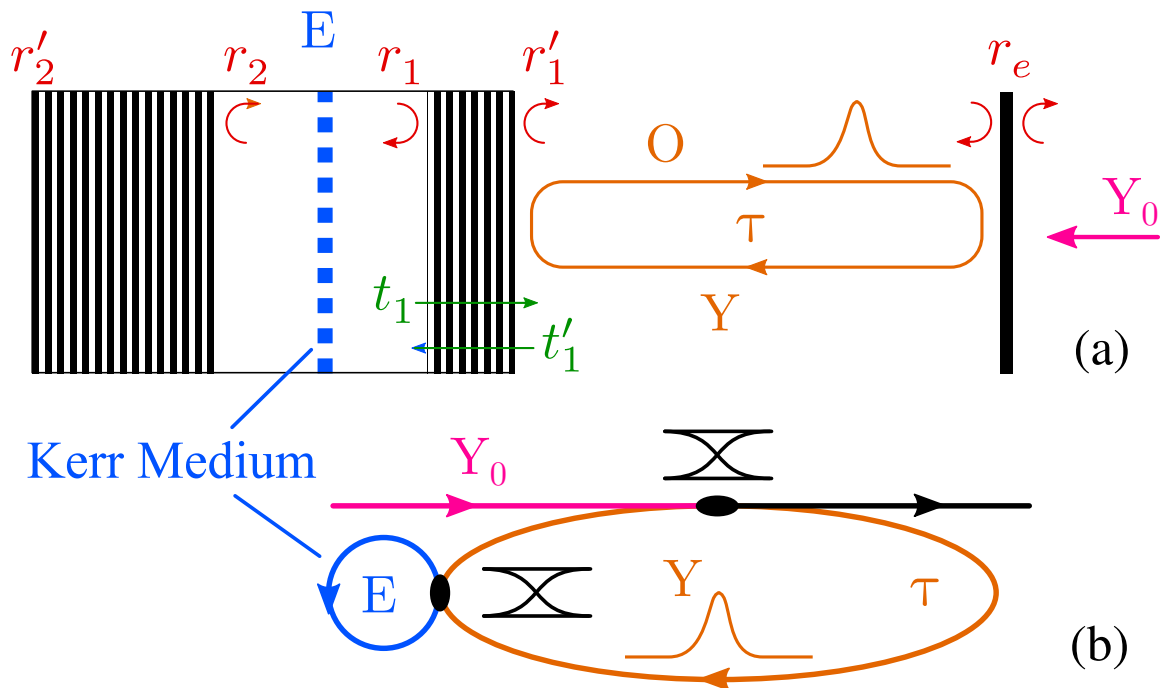


Figure 1: Schematics for different realizations of a micro-cavity with Kerr medium coupled to a large feedback cavity under injection. (a) Planar vertically emitting cavity with feedback mirror. The reflection and transmission coefficients of the mirrors are denoted r_i , r'_i , t_i and t'_i . (b) Whispering gallery mode Kerr micro-cavity coupled to a external feedback ring cavity.

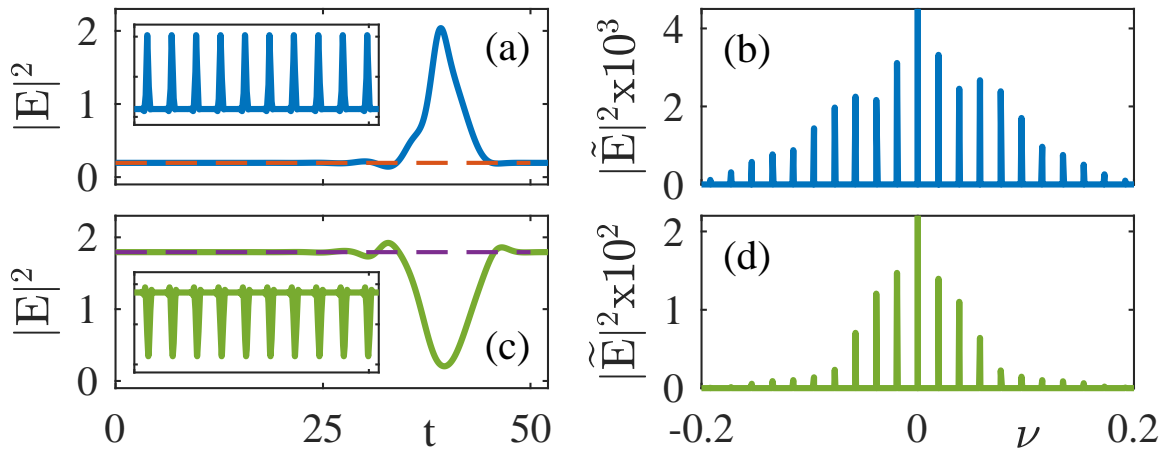


Figure 2: Pulse trains of bright (a) and dark (c) TLSs as a function of time t . The inset shows the dynamics over many round-trips. The respective optical spectra are depicted in panels (b) and (d) where the injection frequency was cut for clarity. Parameters are: $(s, Y_0, \delta, h, \rho_e, \varphi, \tau) = (1, 0.515, 1.5, 2, 0.5, 0, 50)$.

W the width of the nonlinear medium, n_g the group index and c the speed of light. The second term in bracket represents the enhancement of the cavity.

The coupling between E and Y is given in Eq. (2) by a delay algebraic equation (DAE), that takes into account all the multiple reflections in the external cavity. The effects of the external mirror and signal extraction (e.g., a beamsplitter or transmission through the mirror itself) are combined in the attenuation factor $\eta = \rho_e \exp(i\varphi)$, where we defined the effective feedback phase $\varphi = \omega_0\tau + \psi_e$ that combines the accumulated phase per round-trip $\omega_0\tau$ and the phase of the feedback mirror ψ_e . The light coupling efficiency in the cavity is given by the factor $h = (1 + |r_2|)(1 - |r_1|) / (1 - |r_1||r_2|)$. For a perfectly reflecting top mirror $|r_1| = 1$ we have $h = 0$ and no light ever enters the micro-cavity. For $|r_1| = |r_2|$ we have $h = 1$ yielding the balanced Fabry-Perot interferometer. For a perfectly reflecting bottom mirror $|r_2| = 1$, and hence $h = 2$, which corresponds to the imbalanced Gires–Tournois interferometer (GTI) regime. Here, all the photons entering the cavity are eventually reflected back. Yet, as a function of the input frequency, they can exit after a variable amount of round-trips in the micro-cavity, which causes strong dispersive effects. Second and third order dispersion are therefore naturally captured by Eqs. (1,2) [20]. Notice that for coupled ring cavities, a similar model can be derived using [21] as a starting point.

2 Results of numerical simulations

Direct numerical simulations (DNSs) of the system given by Eqs. (1,2) allow to demonstrate the existence of both dark and bright solitons that live on high and low intensity CW backgrounds, respectively. They are presented in Fig. 2 where we show the pulse trains, the detailed temporal profiles, as well as the generated frequency comb. The latter is inversely proportional to the pulse width which is typically in the picosecond range. One can see the leading tail oscillations preceding the main pulse which are due to third order dispersion. GTIs are known for providing tunable second order dispersion off resonance. Yet, at resonance the second order dispersion cancels and as such, the third order contribution becomes dominant. As we operate close to the micro-cavity resonance, third order dispersion leads to strongly asymmetrical soliton profiles. For clarity, the time delay used in Fig. 2 is rather short and only

permits for a few TLSs to coexist. Larger values of τ would induce higher multistability such as in [22]. In conjunction with sufficient detuning δ , the Kerr nonlinearity causes a bistable CW response of the system in a certain range of the injection intensity. We show in Fig. 3a) the resulting hysteresis diagram with the upper CW state in purple and the lower CW state in orange as obtained from DNSs. The gray dotted lines represent the transitions when crossing the folds. In this region sharp transitions between both CW states can be created by appropriate perturbations. These front states are drifting and their

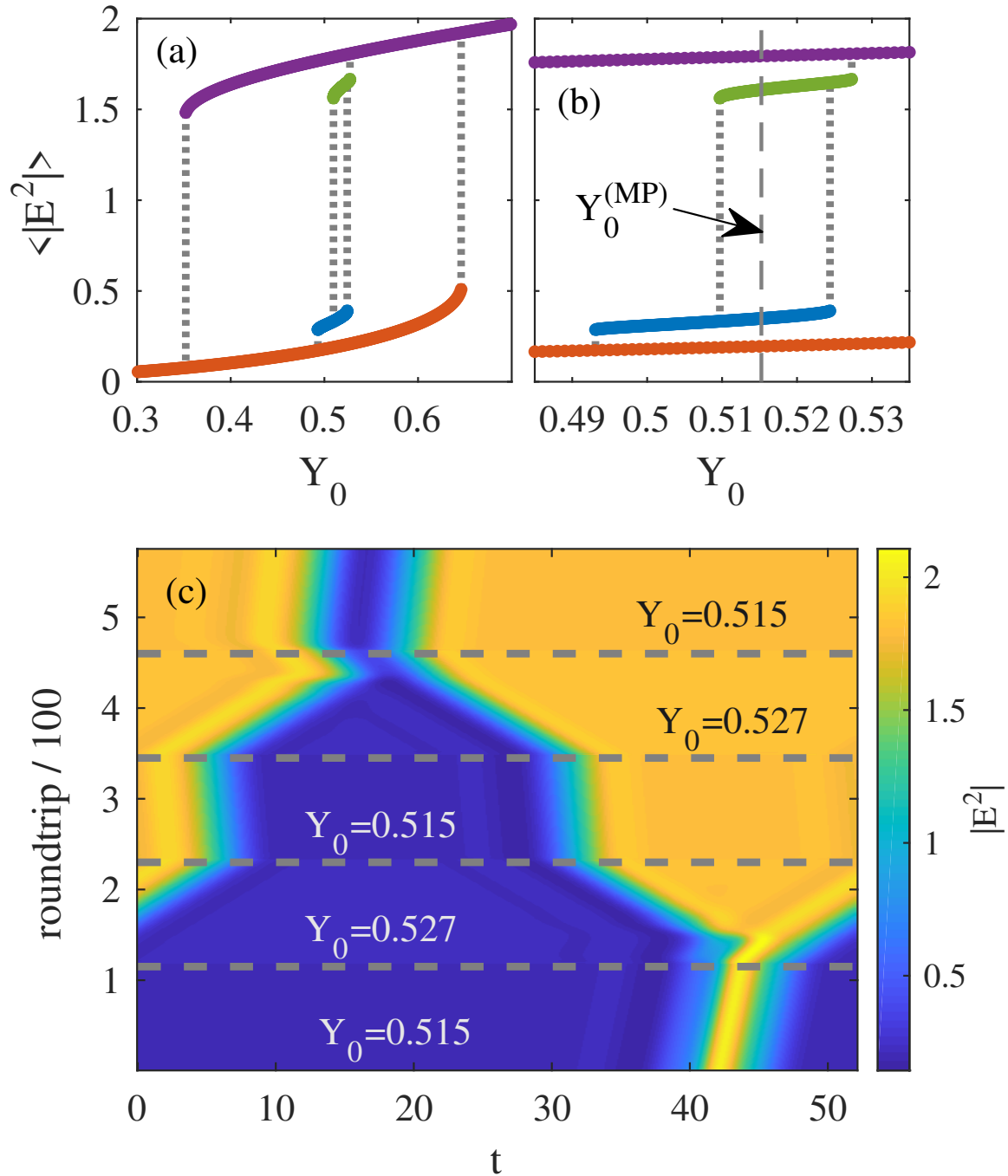


Figure 3: (a) Hysteresis curves of CWs and TLSs obtained from DNSs. (b) Zoom on the TLSs with the MP marked by the vertical dashed line. (c) Space-time representation of the transition from bright to dark TLS via a counter-propagating pair of fronts. Relative front movement is arrested when close to the MP $Y_0^{(MP)} \approx 0.51524$. Other parameters are: $(s, \delta, h, \rho_e, \varphi, \tau) = (1, 1.5, 2, 0.5, 0, 50)$.

speeds generically depend on all parameters. Because of the periodic nature of the cavity, persisting fronts can only be realized as kink/anti-kink pairs. For most parameters, however, they eventually merge into one of the CW states due to their speed difference. For the parameters of Fig. 3, the two types of fronts exhibit the same speed at $Y_0^{(MP)} \approx 0.51524$ where their dynamics is arrested. As in [23], and by analogy with first order phase transitions, we defined this value of Y_0 as the Maxwell point (MP) [24].

Close to the MP the fronts can lock to each other forming the TLSs. Figure 3(b) features a zoom on the region around the MP (dashed gray line) and we depict the average intensity of the dark TLSs in green and the bright TLSs in light blue. The system exhibits hysteresis between the two types of TLSs. By tuning Y_0 outside of the bistable TLS region indicated by the dotted grey lines in Figure 3(b), one observes a transition from dark to bright TLS, or vice versa, that occurs via the following mechanism. First, the TLS breaks up into a pair of fronts connecting the two CW states. Then, these opposed fronts move away from each other, gradually switching the CW background to the opposite state. Finally, the two fronts meet again due to periodic boundary conditions and form the opposite type of TLS. This process is presented as a pseudo space-time diagram in Fig. 3(c) where we change the injection parameter several times during the evolution as indicated by the horizontal dashed gray lines. Notice, how the fronts equilibrate at some large distance from each other when Y_0 is close to the MP.

The CW solution branch underlying the hysteresis can be found analytically and is shown in Fig. 4(a). Linear stability analysis performed in the long delay limit [25] reveals that the unstable part is uniformly unstable whereas both the upper and lower parts are stable for all values of injection. The crossing into the right (unstable) part of the spectrum of a single real eigenvalue coincides with the folds. This crossing is followed by that of conjugated eigenvalue pairs corresponding to a series of Andronov-Hopf (AH) bifurcations. For increasing τ the quasi-continuous spectrum becomes densely filled and the distance between a fold and the closest AH vanishes asymptotically.

We study the TLSs as periodic solutions using the continuation package DDE-BIFTOOL [26]. To that end the DAE as given by Eq. (2) can be transformed into a singularly perturbed DDE

$$\epsilon \dot{Y} = \eta [E(t - \tau) - Y(t - \tau)] - Y + \sqrt{1 + |\eta|^2} Y_0, \quad (3)$$

where we added a singular perturbation parameter ϵ . In the limit of $\epsilon \rightarrow 0$ we approach the original DAE form. Together with a large delay τ the problem becomes very stiff. One has to consider a compromise for the ratio τ/ϵ due to numerical stability limitations. Using $\epsilon = 1/20$ and $\tau = 50$ we achieve excellent agreement with DNS while maintaining DDE-BIFTOOL's full set of capabilities. Alternatively the system (1,2) can be combined into a single neutral delay differential equation (NDDE) that can be treated using an extension for DDE-BIFTOOL [27].

We follow the branch of the single TLS as a function of the injection Y_0 . We present our results in Fig. 4. Panel (a) shows the full bifurcation diagram with the TLS branch line in thick black for stable and thin red for unstable parts. Panel (b) shows a zoom on the area around the MP (vertical dashed gray line). The TLS branch connects the outermost AH points on the uniformly unstable part CW branch, which for $\tau = 50$ virtually coincide with the folds. For both the upper and lower branch, periodic branch emerges supercritically from the unstable CW branch. The latter fold shortly after crossing the MP, thereby gaining stability. This way both dark and bright stable TLSs are created on their respective upper and lower CW backgrounds. Further, these periodic branches then keep folding back and forth around and towards the MP in a collapsing homoclinic snaking scenario [24, 28]. This happens in a qualitatively symmetrical way and both sides converge into a common asymptotic point. Thus, a family of interspersed stable and unstable TLS solutions of varying width connects the upper and lower CW states.

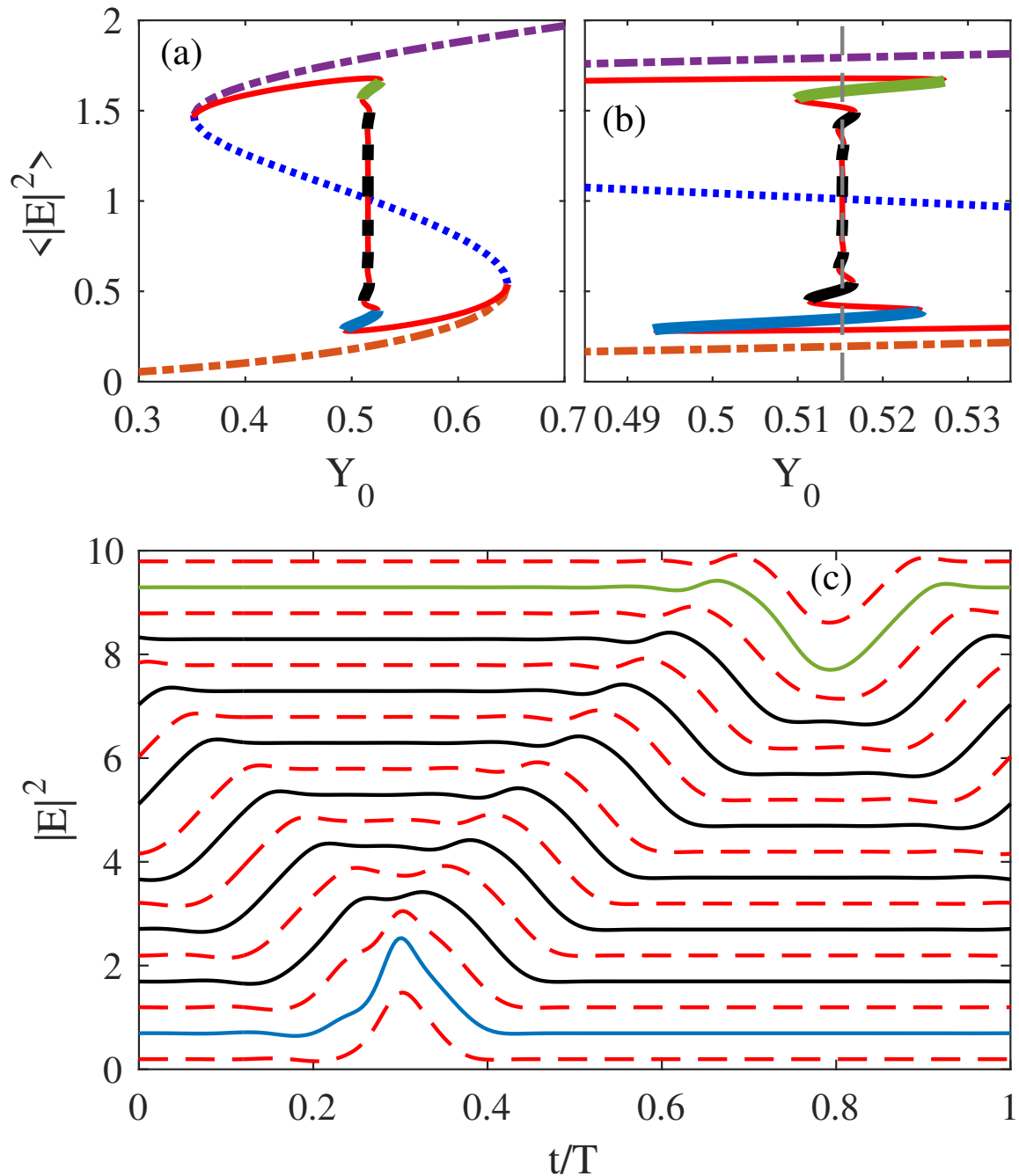


Figure 4: (a) Bifurcation diagram obtained using DDE-BIFTOOL. Stable (unstable) CW solutions in orange/purple dash-dotted (blue dotted). Stable (unstable) TLS periodic branches in thick black (thin red). (b) Zoom on the TLS branch with the MP marked by the vertical dashed line. (c) Stacked solutions along the TLS branch at the MP. Other parameters are: $(s, \delta, h, \rho_e, \varphi, \tau) = (1, 1.5, 2, 0.5, 0, 50)$.

Close to the MP the fronts move slowly with respect to each other. In this situation a pair of fronts can lock together, thereby forming a TLS. Due to third order dispersion the fronts exhibit slowly decaying oscillating tails which induce, via their interactions, a series of preferred distances. This effect is also known as Cherenkov radiation interactions [29]. The stability of such configurations is determined by the interplay between the interaction strength and the tendency of fronts to drift apart due to the deviation from the MP. Closer to the MP the weaker, more distant equilibrium positions stabilize and a transition from bright to dark TLSs occurs. Panel (c) of Fig. 4 shows the periodic solutions at the MP in

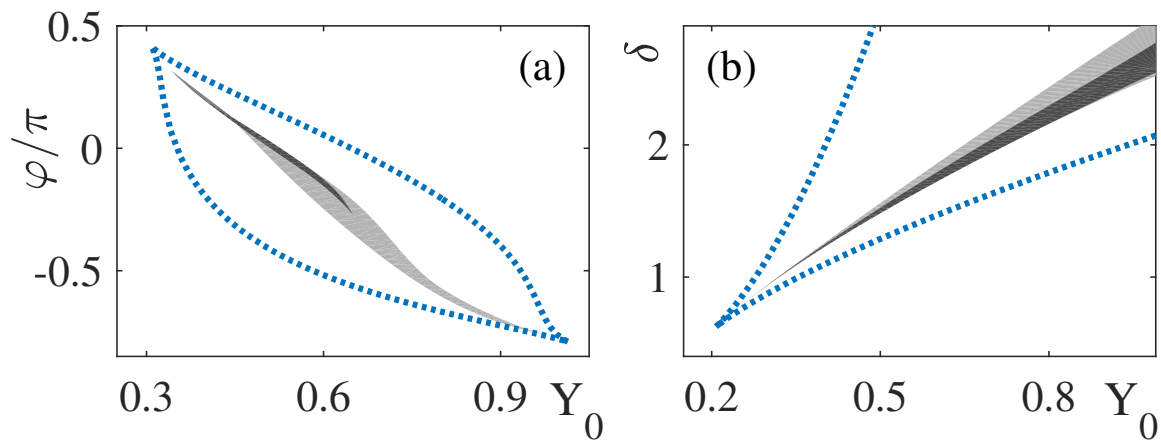


Figure 5: Evolution of the folds limiting the region of CW bistability (dotted blue), fundamental dark TLS (dark gray) and bright TLS (light gray), as a function of (a) (Y_0, φ) and (b) (Y_0, δ) . Other parameters as in Fig. 4.

a stacked arrangement, i.e., the y-axis is for relative comparison only. Solid black stable and dashed red unstable profiles are interspersed as the TLS solution branch in panel (b) folds back and forth. Notice that this mechanism is not limited to a pair of fronts. Close to the MP, multiple front pairs can be arranged into complex temporal patterns by locking the fronts to the various equilibrium distances between them. This is particularly true for larger values of τ . The stability range of these molecule-like structures shrinks for higher order equilibrium distances.

As shown in Fig. 5, TLSs exist in a wide interval of the feedback phase and of the cavity detuning. We note the asymmetry between the region of stable existence for dark and bright TLSs. With decreasing $\varphi < -0.1$ a Turing instability develops on the upper CW solution that gradually invades the whole branch, first preventing dark TLSs, later inducing oscillations on the trailing edge of bright TLSs, and finally fully dominating the dynamics of the system. Multi-hump solutions follow the same trend. In addition, small deviations from the perfect GTI case $h = 2$ do not impact the dynamics. On the other hand, stronger feedback from the external mirror, i.e. $|\eta| \rightarrow 1$, diminishes the damping of the leading tail thereby increasing the interaction strength between fronts. As a result, the TLS region becomes wider yet at the same time the multistability increases, making the bifurcation structure very intricate. We therefore chose a relatively low value of η that yields a clear cut bifurcation diagrams explaining the underlying phenomenon. We also note that both intensity and phase modulation of the injection beam provide for a way of perturbing the system to write TLSs. Finally, besides TLSs and domain walls (fronts), the system exhibits square waves with period $T \simeq 2\tau$, e.g., as in [23, 30], for feedback phases around $\varphi = \pi$. These interesting topics are out of the scope of the current manuscript.

3 Conclusion

In summary, we presented a new setup that consists of an imbalanced micro-cavity operating in the Gires–Tournois regime, filled with Kerr nonlinearity and coupled to an external cavity under CW injection. Hysteresis between sets of dark and bright TLSs of different widths was disclosed and their formation scenario was unveiled using bifurcation analysis. Connecting fronts between bistable CW background states can lock to each other at various positions due to the strongly oscillating tails induced by third order dispersion. We believe this setup to be interesting for applications as it offers the possibility to generate complex temporal patterns and frequency combs while being tunable in repeti-

tion rate. Finally, high optical power can be achieved by harnessing the transverse profile of the field in the cavity.

References

- [1] A. C. Tropper, H. D. Foreman, A. Garnache, K. G. Wilcox, and S. H. Hoogland, "Vertical-external-cavity semiconductor lasers," *J. Phys. D: Appl. Phys.*, vol. 37, pp. R75–R85, 2004.
- [2] A. Laurain, M. Myara, G. Beaudoin, I. Sagnes, and A. Garnache, "Multiwatt—power highly—coherent compact single—frequency tunable vertical—external—cavity—surface—emitting—semiconductor—laser," *Opt. Express*, vol. 18, pp. 14627–14636, Jul 2010.
- [3] F. Leo, S. Coen, P. Kockaert, S.-P. Gorza, P. Emplit, and M. Haelterman, "Temporal cavity solitons in one-dimensional Kerr media as bits in an all-optical buffer," *Nature Photonics*, vol. 4, pp. 471 EP –, May 2010. Article.
- [4] T. Herr, V. Brasch, J. D. Jost, C. Y. Wang, N. M. Kondratiev, M. L. Gorodetsky, and T. J. Kippenberg, "Temporal solitons in optical microresonators," *Nature Photonics*, vol. 8, pp. 145 EP –, Dec 2013. Article.
- [5] A. Coillet, I. Balakireva, R. Henriët, K. Saleh, L. Larger, J. M. Dudley, C. R. Menyuk, and Y. K. Chembo, "Azimuthal Turing patterns, bright and dark cavity solitons in Kerr combs generated with whispering-gallery-mode resonators," *IEEE Photonics Journal*, vol. 5, pp. 6100409–6100409, Aug 2013.
- [6] V. Lobanov, G. Lihachev, T. J. Kippenberg, and M. Gorodetsky, "Frequency combs and platicons in optical microresonators with normal gvd," *Opt. Express*, vol. 23, pp. 7713–7721, Mar 2015.
- [7] C. Godey, I. V. Balakireva, A. Coillet, and Y. K. Chembo, "Stability analysis of the spatiotemporal Lugiato-Lefever model for Kerr optical frequency combs in the anomalous and normal dispersion regimes," *Phys. Rev. A*, vol. 89, p. 063814, Jun 2014.
- [8] X. Xue, Y. Xuan, Y. Liu, P.-H. Wang, S. Chen, J. Wang, D. E. Leaird, M. Qi, and A. M. Weiner, "Mode-locked dark pulse Kerr combs in normal-dispersion microresonators," *Nature Photonics*, vol. 9, pp. 594 EP –, Aug 2015. Article.
- [9] B. Garbin, Y. Wang, S. G. Murdoch, G.-L. Oppo, S. Coen, and M. Erkintalo, "Experimental and numerical investigations of switching wave dynamics in a normally dispersive fibre ring resonator," *The European Physical Journal D*, vol. 71, p. 240, Sep 2017.
- [10] N. N. Rosanov, "I Transverse patterns in wide-aperture nonlinear optical systems," vol. 35 of *Progress in Optics*, pp. 1 – 60, Elsevier, 1996.
- [11] P. Parra-Rivas, D. Gomila, E. Knobloch, S. Coen, and L. Gelens, "Origin and stability of dark pulse Kerr combs in normal dispersion resonators," *Opt. Lett.*, vol. 41, pp. 2402–2405, Jun 2016.
- [12] P. Parra-Rivas, E. Knobloch, D. Gomila, and L. Gelens, "Dark solitons in the Lugiato-Lefever equation with normal dispersion," *Phys. Rev. A*, vol. 93, p. 063839, Jun 2016.

- [13] G.-L. Oppo, A. J. Scroggie, and W. J. Firth, “From domain walls to localized structures in degenerate optical parametric oscillators,” *Journal of Optics B: Quantum and Semiclassical Optics*, vol. 1, pp. 133–138, Jan 1999.
- [14] P. Parra-Rivas, L. Gelens, T. Hansson, S. Wabnitz, and F. Leo, “Frequency comb generation through the locking of domain walls in doubly resonant dispersive optical parametric oscillators,” *Opt. Lett.*, vol. 44, pp. 2004–2007, Apr 2019.
- [15] A. Pimenov, S. Amiranashvili, and A. G. Vladimirov, “Temporal cavity solitons in a delayed model of a dispersive cavity ring laser,” *WIAS Preprint 2581 (accepted to Mat. Mod. of Nat. Phen.)*, Mar 2019.
- [16] M. Tlidi and L. Gelens, “High-order dispersion stabilizes dark dissipative solitons in all-fiber cavities,” *Opt. Lett.*, vol. 35, pp. 306–308, Feb 2010.
- [17] P. Parra-Rivas, D. Gomila, and L. Gelens, “Coexistence of stable dark- and bright-soliton Kerr combs in normal-dispersion resonators,” *Phys. Rev. A*, vol. 95, p. 053863, May 2017.
- [18] J. H. Talla Mbé, C. Milián, and Y. K. Chembo, “Existence and switching behavior of bright and dark Kerr solitons in whispering-gallery mode resonators with zero group-velocity dispersion,” *The European Physical Journal D*, vol. 71, p. 196, Jul 2017.
- [19] J. Mulet and S. Balle, “Mode locking dynamics in electrically-driven vertical-external-cavity surface-emitting lasers,” *Quantum Electronics, IEEE Journal of*, vol. 41, no. 9, pp. 1148–1156, 2005.
- [20] C. Schelte, P. Camelin, M. Marconi, A. Garnache, G. Huyet, G. Beaudoin, I. Sagnes, M. Giudici, J. Javaloyes, and S. Gurevich, “Third order dispersion in time-delayed systems,” *Physical review letters*, vol. 123, no. 4, p. 043902, 2019.
- [21] R. M. Arhipov, A. Amann, and A. G. Vladimirov, “Pulse repetition-frequency multiplication in a coupled cavity passively mode-locked semiconductor lasers,” *Applied Physics B*, vol. 118, pp. 539–548, Mar 2015.
- [22] M. Marconi, J. Javaloyes, S. Balle, and M. Giudici, “How lasing localized structures evolve out of passive mode locking,” *Phys. Rev. Lett.*, vol. 112, p. 223901, Jun 2014.
- [23] J. Javaloyes, T. Ackemann, and A. Hurtado, “Arrest of domain coarsening via anti-periodic regimes in delay systems,” *Phys. Rev. Lett.*, vol. 115, p. 223901, Nov 2015.
- [24] J. Burke and E. Knobloch, “Homoclinic snaking: Structure and stability,” *Chaos: An Interdisciplinary Journal of Nonlinear Science*, vol. 17, no. 3, p. 037102, 2007.
- [25] S. Yanchuk and M. Wolfrum, “A multiple time scale approach to the stability of external cavity modes in the Lang-Kobayashi system using the limit of large delay,” *SIAM Journal on Applied Dynamical Systems*, vol. 9, no. 2, pp. 519–535, 2010.
- [26] K. Engelborghs, T. Luzyanina, and D. Roose, “Numerical bifurcation analysis of delay differential equations using dde-biftool,” *ACM Trans. Math. Softw.*, vol. 28, pp. 1–21, Mar. 2002.
- [27] D. A. W. Barton, B. Krauskopf, and R. E. Wilson, “Collocation schemes for periodic solutions of neutral delay differential equations,” *Journal of Difference Equations and Applications*, vol. 12, no. 11, pp. 1087–1101, 2006.

- [28] J. Knobloch and T. Wagenknecht, "Homoclinic snaking near a heteroclinic cycle in reversible systems," Physica D: Nonlinear Phenomena, vol. 206, no. 1, pp. 82 – 93, 2005.
- [29] A. G. Vladimirov, S. V. Gurevich, and M. Tlidi, "Effect of Cherenkov radiation on localized-state interaction," Phys. Rev. A, vol. 97, p. 013816, Jan 2018.
- [30] M. Nizette, "Stability of square oscillations in a delayed-feedback system," Phys. Rev. E, vol. 70, p. 056204, Nov 2004.